antioxidants

MDPI

Article

Reassessing Whether Biodegradable Microplastics Are Environmentally Friendly: Differences in Earthworm Physiological Responses and Soil Carbon Function Impacts

Yuze Li, Dongxing Zhou, Hongyan Wang, Wenfei Zhu, Rui Wang and Yucui Ning *

College of Resources and Environment, Northeast Agricultural University, Harbin 150030, China; s230201030@neau.edu.cn (Y.L.); zhouboshi@neau.edu.cn (D.Z.); s240201055@neau.edu.cn (H.W.); s240201059@neau.edu.cn (W.Z.); s240202099@neau.edu.cn (R.W.)

* Correspondence: yucuining@neau.edu.cn

Abstract

Biodegradable plastics are not a primary solution to plastic pollution, and empirical evidence on whether they are environmentally friendly remains lacking. In this study, we systematically compared the toxic effects of traditional microplastics (polypropylene, PP; polystyrene, PS) with biodegradable microplastics (polylactic acid, PLA; polyhydroxyalkanoates, PHA) on the haplic phaeozem ecosystem. Through mathematical modeling analysis, it was found that earthworms initially rely on antioxidant enzymes to resist stress, mid-term activation of detoxifying enzymes to repair damage, and maintaining physiological balance through metabolic regulation and immune enhancement in later stages. We elucidated their mechanism differences: PLA and PP caused severe damage to the antioxidant system and cell membrane, with PLA mainly relying on POD to clear peroxides and PP relying on GST. In addition, PLA and PS can induce early neurotoxicity (AChE), while PHA induces late neurotoxicity. Furthermore, this study provides direct evidence proving that biodegradable microplastics are not environmentally friendly by breaking through the one-way research framework of "microplastic biotoxicity" and innovatively constructing a path analysis model that links biological physiological responses with soil ecological functions. We also provide a scientific basis to evaluate the ecological risks of microplastic pollution in soil and the whether biodegradable plastics are truly environmentally friendly.

Keywords: microplastics; *Eisenia fetida*; haplic phaeozem; factor analysis; principal component analysis; path analysis

check for updates

Received: 22 August 2025
Revised: 23 September 2025
Accepted: 29 September 2025
Published: 1 October 2025

Citation: Li, Y.; Zhou, D.; Wang, H.; Zhu, W.; Wang, R.; Ning, Y. Reassessing Whether Biodegradable Microplastics Are Environmentally Friendly: Differences in Earthworm Physiological Responses and Soil Carbon Function Impacts. *Antioxidants* **2025**, *14*, 1197. https://doi.org/10.3390/antiox14101197

Copyright: © 2025 by the authors. Licensee MDPI, Basel, Switzerland. This article is an open access article distributed under the terms and conditions of the Creative Commons Attribution (CC BY) license (https://creativecommons.org/licenses/by/4.0/).

1. Introduction

Since the first successful synthesis in 1907, plastics have been widely utilized across various industries due to their low production cost, high plasticity, and stable chemical properties [1]. However, a large amount of plastic waste is improperly managed. Under the influence of ultraviolet radiation, microbial degradation, mechanical abrasion, and other environmental factors, unrecycled plastics gradually fragment into particles smaller than 5 mm in diameter [2], known as microplastics (MPs). Among these, polyethylene (PE), polypropylene (PP), and polystyrene (PS) are the most common [3]. With the long-term and continuous accumulation of these microplastics in the soil, they will not only have a negative impact on soil structure, but also hinder nutrient cycling, reduce water retention capacity, and pose serious threats to soil biota [4], making them a pressing global environmental concern [5].

To mitigate the environmental risks associated with traditional microplastics, the draft of the Global Plastics Treaty [6] indicates that biodegradable plastics may serve as a potential means to end plastic pollution. This perspective, coupled with the continuous growth of human demand for plastics, has led to the global production of biodegradable plastics reaching 2.47 million tons in 2024, with a projected increase to 5.73 million tons by 2029 [7]. Biodegradable microplastics ultimately degrade carbon dioxide and water, and are therefore labeled as "eco-friendly" materials [8]. However, whether biodegradable microplastics are truly environmentally friendly, especially in soil ecosystems, lacks empirical evidence. Considering that pollution remediation is very difficult, the EU is very cautious about the use of biodegradable materials. Therefore, the Single-Use Plastics Directive [9] passed by the European Union in June 2019 imposes restrictions on some oxygen-containing biodegradable plastic products. The implementation guidance document for this directive, released in May 2021, further clarifies that biodegradable plastics or biobased plastics still belong to the category "plastics" and cannot be marked as "biodegradable" when used in disposable products. This has also raised concerns about the concept of "biodegradability".

Earthworms are among the most common invertebrates in soil ecosystems. Through their feeding and burrowing activities, they facilitate the decomposition of organic matter, enhance soil porosity, and improve the soil's capacity to retain water and nutrients. As such, they are often referred to as "ecosystem engineers" of the soil [10,11]. Due to their widespread distribution, low trophic level, and high exposure potential to environmental contaminants, earthworms are commonly used as bioindicators for assessing soil pollution and environmental quality, effectively reflecting the toxicological impacts of pollutants on terrestrial ecosystems [12].

However, earthworms have numerous response indicators after stress, and when using traditional biostatistics for data analysis, it is necessary to encompass the entire physiological and biochemical processes of the organism. As a result, the experimental content is numerous, the process is complex, and the credibility of the data analysis results is often poor [13]. At the same time, a single mathematical model suffers from excessive loss of information during data extraction, loss of biological significance of data in analysis results, and inaccurate judgment matrices due to the excessive increasing workload [14]—and is sometimes even unable to correctly explain the biological significance of the model [15]. Therefore, in the ecological toxicology research of earthworms, there is an urgent need for a combined model of principal component analysis and factor analysis to achieve accurate and scientific screening of biomarkers, in order to assist in the ecological safety evaluation and bioremediation research of polluted soil.

In this context, the present study employed *Eisenia fetida* as the model organism to investigate the oxidative stress responses induced by exposure to four types of microplastics: PP, PS, PLA (polylactic acid), and PHA (polyhydroxyalkanoates). An innovative "progressive factor analysis principal component analysis model" is used to identify key sensitive oxidative stress biomarkers of earthworms exposed to microplastics, thereby elucidating their survival strategies in soil contaminated with microplastics. In addition, the path analysis method is used to link biological physiological responses with soil ecological functions to clarify whether biodegradable microplastics are truly environmentally friendly.

2. Materials and Methods

2.1. Characterization of Microplastics

The microplastics used in this study, PP, PS, PLA, and PHA, were 200 mesh (75 μm ± 10 μm) powders supplied by Zhongxin Plastic Co., Ltd., Guangzhou, China. The chemical structure of the microplastics was confirmed using a Raman spectrometer (inVia, Renishaw, Gloucestershire, UK) with a laser wavelength of 785 nm and a wavenum-

ber range of 200–3000 cm^{-1}. After the microplastics were sputter-coated with gold, their morphologies were observed using a scanning electron microscope (SU8010, Hitachi, Tokyo, Japan).

2.2. Test Reagents

Phosphate-buffered saline (PBS, dry powder) was purchased from Coolable Technology Co., Ltd., Beijing, China (analytical grade). Each packet was diluted with ultrapure water to a final volume of 1 L, with a pH of 7.2–7.4. The final buffer composition included 137 mM NaCl, 2.7 mM KCl, 10 mM Na_2HPO_4, and 2 mM KH_2PO_4. Medical-grade normal saline was obtained from local pharmacies.

2.3. Test Soil

The test soil was black soil that was collected from the experimental fields of Northeast Agricultural University (pH: 7.65; organic matter: 17.36%); total nitrogen: 0.901%). Fresh topsoil samples (0–20 cm depth) were collected, and plant debris, stones, and other impurities were removed. The soil was air dried and sieved through a 5 mm mesh. Semi-decomposed cow dung was used as an earthworm feed source, mixed with the soil at a ratio of 7:3 (*w*/*w*) (black soil:cow dung) (microplastic: 0.05 mg/kg, cadmium; lead; nickel: <0.01 mg/kg). The moisture content was adjusted to 40% of the soil's maximum water holding capacity using deionized water, following OECD guidelines [16,17]. The cow dung was prepared by natural air drying, grinding, and sieving through a 5 mm mesh.

2.4. Tested Earthworms

The test organism, *Eisenia fetida*, was sourced from a national ecological farm. Healthy adult earthworms, over 2 months old, with well-developed clitella and weighing between 300 and 500 mg, were selected. Prior to the experiment, earthworms were rinsed with clean water to remove surface debris and residual feed. After drying with filter paper, they were placed on moist filter paper in a dark environment for 24 h to purge intestinal contents.

2.5. Experimental Design

Based on the results of preliminary experiments and previous research findings [18–21], four microplastic types (PP, PS, PLA, and PHA) were tested at concentrations of 0, 100, 500, 1000, and 1500 mg/kg. Each treatment was replicated five times. The exposure test was conducted in a 1000 mL wide-mouthed bottle, each containing 120 g of treated test soil mixed thoroughly with the respective concentration of microplastics. Five depurated earthworms were placed in each flask. The flasks were covered with plastic film to prevent moisture loss and incubated in a controlled artificial climate chamber at (20 ± 2) °C, 80% relative humidity, and in complete darkness.

2.6. Sample Collection

According to the sampling requirements of weekly intervals in the OECD guidelines [16], the experimental period lasted 35 days. One earthworm was randomly selected from each flask every 7 days (take a total of 5 earthworms each time). After collection, the earthworm's surface was rinsed with deionized water and gently dried using filter paper. The sample was then transferred to a glass homogenizer, and phosphate-buffered saline (PBS, pH 7.3) was added at a ratio of 1:9 (*w*/*v*, accurate to 0.0001 g) for homogenization. The resulting homogenate was transferred to a centrifuge tube and centrifuged at 4000 r/min for 10 min at 4 °C. The supernatant was collected and stored at −20 °C for subsequent biochemical analysis. An amount of 10 g soil was taken from each bottle every 7 days, air-dried naturally, ground and then sieved through a 200 mesh sieve for the determination of total soil carbon.

2.7. Determination of Enzyme Indexes

Frozen supernatant samples were thawed at +4 °C prior to analysis. The following biochemical parameters were determined using standard protocols: the total protein content was determined by Coomassie Brilliant Blue Colorimetry [22]; peroxidase (POD) activity was assessed based on the catalytic reaction of POD with hydrogen peroxide [23]; superoxide dismutase (SOD) activity was determined via its specific inhibitory effect on superoxide anion radicals [24]; glutathione peroxidase (GPX) activity was measured using 2-thio-2,4-dinitrobenzoic acid colorimetry [25]; glutathione-S-transferase (GST) activity was evaluated by 1-chloro-2,4-dinitrobenzene colorimetry [26]; catalase (CAT) activity was determined using ammonium molybdate colorimetry [27]; malondialdehyde (MDA) content was measured via the thiobarbituric acid (TBA) method [28]; acetylcholinesterase (AChE) activity was analyzed using 1,3,5-trinitrobenzene colorimetry [29]. Soil total carbon (TC) was measured using the combustion method [30].

2.8. Data Analysis

2.8.1. Factor Analysis

Factor analysis is a multivariate statistical method that reduces dimensionality by transforming multiple index variables into a few comprehensive factors [14,31]. To minimize the impact of variability among oxidative stress indicators, the original data were normalized and expressed as the percentage change in each test group relative to the sum across all groups:

$$U = \frac{x_s}{\sum_{s=1}^{t} x_{st}} \times 100\%$$

Here, x_S represents the oxidative stress indicators, including POD, SOD, CAT, MDA, AChE, GPX, and GST; t represents the number of samples.

After dimensionality reduction, the n biological markers can be represented as a linear combination of m common factors (m < n), denoted as $F1, F2, \ldots Fm$. The construction process of the model refers to the research of Zhou et al. [32].

All statistical analyses were conducted using SPSS software version 19.0.

2.8.2. Principal Component Analysis

Principal component analysis (PCA) [33] is a multivariate statistical method used to explore correlations among multiple variables. PCA identifies the internal structure of complex datasets by transforming them into a smaller set of uncorrelated principal components, thereby simplifying data interpretation [34]. In this study, PCA was applied to analyze the oxidative stress response of earthworms under microplastic exposure. The index matrices of the experimental group and the control group were denoted as X_f and X, respectively:

$$X_f = \begin{Bmatrix} x_{11} & x_{12} & \cdots & x_{1g} \\ x_{21} & x_{22} & \cdots & x_{2g} \\ \cdots & \cdots & \cdots & \cdots \\ x_{n1} & x_{n2} & \ldots & x_{ng} \end{Bmatrix} \quad X_0 = \begin{Bmatrix} x_{01} & x_{02} & \cdots & x_{0n} \\ x_{01} & x_{02} & \cdots & x_{0n} \\ \cdots & \cdots & \cdots & \cdots \\ x_{01} & x_{02} & \cdots & x_{0n} \end{Bmatrix}$$

The variable sample matrix is then obtained as: $\Delta X = X_f - X_0$

In this context, f is the stress time; g is the number of samples, which is the concentration of microplastic stress; n is the number of oxidative stress indicators, including POD, SOD, CAT, MDA, AChE, GPX, and GST, measured in earthworms exposed to microplastic-contaminated soil. To reduce dimensionality while minimizing squared error in the sample set, coordinate transformation was applied using the Jacobi method to compute the orthog-

onal transformation matrix. A total of m principal components were then extracted, where $m < n$. The Z-score method is used for standardization (Appendix A for detailed process)

$$C^{n}_{\eta=1} = \varepsilon_{\eta 1}X_{j1} + \varepsilon_{\eta 2}X_{j2} + \cdots + \varepsilon_{\eta n}X_{jn},\ S^{n}_{\eta=1} = \left|\sum\nolimits_{\eta=1}^{m} C^{n}_{\eta j}\xi_{\eta}\right|$$

All data processing and statistical analysis were conducted using SPSS software version 19.0.

2.8.3. Path Analysis

After the occurrence of microplastic stress, the oxidative stress index in earthworms is used as the independent variable X_i and the total carbon content of soil was the dependent variable Y. A path analysis model was constructed in order to analyze the relationship between biological physiological responses and soil ecological functions in microplastic-polluted environments, where

r_{ij} represents the simple correlation coefficient between x_i and x_j; r_{ij} represents the correlation coefficient between x_i and y; P_{ij} is the direct path coefficient, which represents the magnitude of x_i directly acting on Y when other variables are fixed. Additionally, r_{ij} was decomposed into the following system of equations:

$$\begin{cases} r_{1y} = P_{1y} + P_{2y}r_{12} + P_{3y}r_{13} + \cdots + P_{ny}r_{1n} \\ r_{2y} = P_{2y} + P_{1y}r_{21} + P_{3y}r_{23} + \cdots + P_{ny}r_{2n} \\ \cdots \\ r_{iy} = P_{iy} + \sum_{j\neq 1} P_{jy}r_{ij}(i = 1, 2, \cdots, n) \\ \cdots \\ r_{ny} = P_{ny} + P_{1y}r_{n1} + P_{2y}r_{n2} + \cdots + P_{(n-1)y}r_{n(n-1)} \end{cases}$$

The remaining diameter coefficient must be ≤ 0.25.

3. Results and Discussion

3.1. Characteristics of Microplastics

As shown in Figure 1, the surfaces of PP and PS are smooth and flat, with intact edges, and without obvious pores, rough protrusions or agglomeration phenomena, and their overall morphologies are neat and concise. A part of the PLA surface has a rough texture, and even has porous or uneven structures. PHA presents rod-shaped or fibrous aggregation structures—not in granular form, but forms clusters composed of slender structures. Raman spectroscopy was used to identify the characteristic peaks of microplastics in the range of 200–3000 cm^{-1}. As shown in Figure 2, PP exhibited characteristic peaks at 809, 842, 974, 1153, 1331 and 1461 cm^{-1}, corresponding to distinct molecular vibrations [35]. Specifically, the peaks at 809 and 842 cm^{-1} are attributed to C-H rocking vibrations, 974 cm^{-1} to asymmetric C-C stretching, 1153 and 1331 cm^{-1} to C-C stretching vibrations, and 1461 cm^{-1} to C-H bending vibrations [36]. PS showed characteristic peaks at 621, 792, 1002, 1156, 1445, and 1604 cm^{-1}, respectively [37]. Among these, the peaks at 621, 792 and 1445 cm^{-1} correspond to C-C stretching vibrations, while the peak at 1604 cm^{-1} is associated with C-H stretching in the benzene ring [38,39]. Notably, the peak at 1002 cm^{-1}, representing the ring breathing mode of the benzene ring, was the most prominent and is commonly used as a diagnostic peak for PS identification [40].

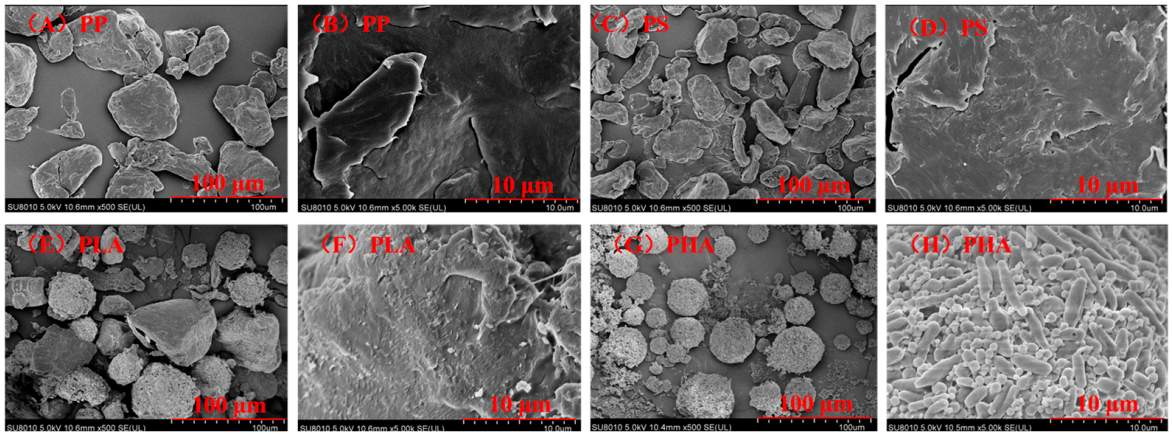


Figure 1. SEM images of four types of microplastics ((**A**,**C**,**E**,**G**): 500; (**B**,**D**,**F**,**H**): 5000).

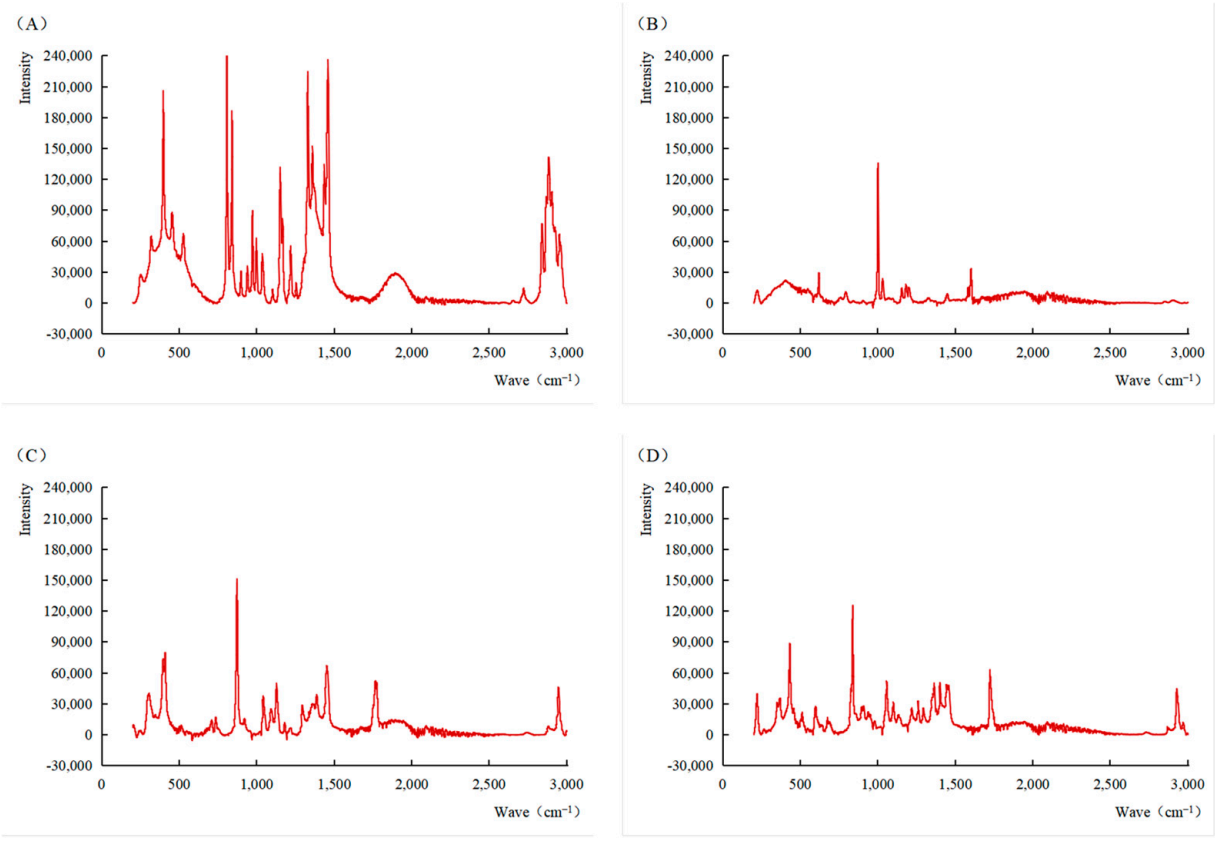


Figure 2. Raman spectra of four types of microplastics. ((**A**): PP; (**B**): PS; (**C**): PLA; (**D**): PHA).

For polylactic acid (PLA), a peak at 411 cm^{-1} was assigned to C=O deformation vibration, and the peak at 874 cm^{-1} was due to the (C-COO) stretching of the polymer chain repeat units. Additional peaks at 1044, 1129, and 1453 cm^{-1} corresponded to C-CH_3 stretching, CH_3 in-plane bending, and CH_3 asymmetric bending, respectively. The peak at 1767 cm^{-1} indicated C=O stretching, while the strong peak at 2948 cm^{-1} was attributed to symmetric CH_3 stretching [41]. PHA showed characteristic peaks at 839, 1059, 1366, and 1725 cm^{-1}. The peak at 839 cm^{-1} was related to C-COO stretching, 1059 cm^{-1} to C-C stretching, and 1366 cm^{-1} to C-H rocking vibrations. The peak at 1725 cm^{-1}, associated with C=O stretching, served as a key marker for identifying PHA [42].

3.2. Physiological Response of Earthworms Under Microplastic Stress

3.2.1. Oxidative Stress Effects in Earthworms

As shown in Figure 3, under PP stress, the activities of most antioxidant enzymes in *Eisenia fetida* peaked at a concentration of 500 mg/kg and subsequently declined with increasing concentration. Specifically, at 500 mg/kg, the maximum SOD activity was observed on the 28th day of stress, at 97.62 U/mg prot; the maximum GPX activity was detected on the 21st day of stress, at 183.66 U/mg prot; and the maximum AChE activity was noted on the 21st day of stress. At this concentration (500 mg/kg), AChE activity gradually decreased with the passage of time. Under different stress concentrations and exposure times, the CAT activity of the PP treatment group was lower than that of the control group (CK).

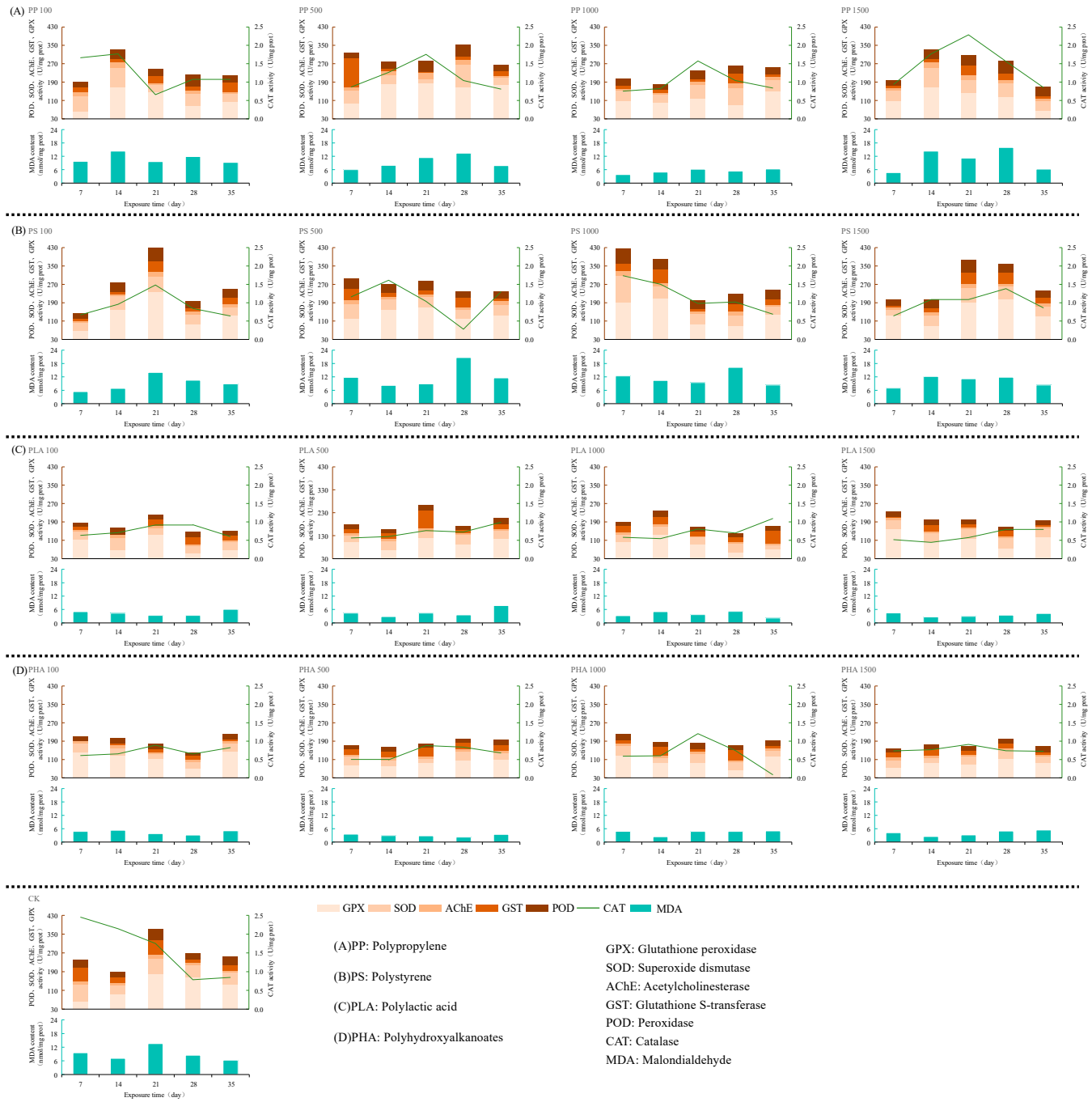


Figure 3. Oxidative stress effect of earthworm under four kinds of microplastic stress.

Under PS stress (Figure 3), enzyme activities generally increased at 1000 mg/kg, but declined significantly at 1500 mg/kg. POD and SOD reached their highest activities, 66.02 and 113.16 U/mg prot, respectively, on day 7 under 1000 mg/kg stress, followed by a gradual decrease at higher concentrations. GST activity peaked at 63.16 U/mg prot on the 14th day under 1000 mg/kg of PS stress. However, GST activity dropped sharply to 4.89 U/mg prot at 1500 mg/kg.

For PLA stress (Figure 3), most enzyme activities reached their maximum at low concentrations (100 and 500 mg/kg). For example, the peak activities of POD, SOD, and AChE were observed at 100 mg/kg on the 7th day of PLA stress. However, with increasing PLA stress concentration, the activities of POD, SOD, and AChE exhibited a decreasing trend.

Under PHA stress (Figure 3), most enzyme activities reached their peak at 1000 mg/kg of PHA stress. The activities of CAT, SOD, AChE, and GST reached their maximum values at 1000 mg/kg of PHA stress (1.2, 43.65, 12.93, and 47.44 U/mg prot, respectively), and then decreased with increasing PHA concentration. With the passage of time under this concentration (1000 mg/kg of PHA stress), the activities of CAT, AChE, and GST gradually decreased. In contrast, SOD activity exhibited a trend of first decreasing and then increasing at this concentration.

Overall, except for GST activity under PLA stress and GPX activity under PHA stress, all other enzyme activities under PS, PLA, and PHA stress were lower than those in the CK. Both traditional and biodegradable microplastics could inhibit the enzyme activities in earthworms through oxidative stress [43].

3.2.2. Screening of Sensitive Oxidative Stress Indicators

A factor analysis model was constructed to evaluate the comprehensive eigenvalues, contribution rates, and factor loadings of oxidative stress indicators under different microplastic types and exposure durations. Based on this analysis, the key oxidative stress biomarkers in earthworms were identified (Table 1). Upon exposure to microplastic stress, large quantities of O_2^- were generated in *Eisenia fetida*, disrupting the organism's oxidative stress balance [44]. As shown in Table 1, the total protein content an indicator of metabolic activity fluctuated significantly under oxidative stress. SOD, which catalyzes the dismutation of O_2^- into H_2O_2 and molecular oxygen (O_2), plays a critical initial role in the antioxidant defense system [45]. Since H_2O_2 remains biologically harmful, it must be further decomposed. CAT and POD are key enzymes responsible for the breakdown of H_2O_2 into water and oxygen [46]. Accordingly, during the early phase of microplastic stress (day 7), SOD, POD, and CAT were identified as the most sensitive oxidative stress biomarkers (Table 1).

Table 1. Screening of sensitive oxidative stress indicators at different stress stages.

Stress Test Group	Stress Time Day				
	7	**14**	**21**	**28**	**35**
PP	SOD	MDA	POD	MDA	GST
PS	POD	AChE	SOD	SOD	AChE
PLA	CAT	GPX	POD	POD	POD
PHA	POD	POD	AChE, MDA	AChE	SOD

Reactive oxygen species (ROS) also induced lipid peroxidation, resulting in the formation of MDA, a commonly used biomarker for assessing oxidative damage to cell membranes [47]. In this study, MDA was identified as the primary oxidative stress indicator under PP exposure on days 14 and 28. As shown in Figure 3, MDA levels increased initially

with stress duration, peaking on day 28 before declining. These results suggest that lipid peroxidation began on day 14 and intensified over time, reaching a maximum on day 28, followed by a potential recovery or enzyme-mediated mitigation. Similar findings have been reported in *Eisenia fetida* exposed to LDPE and PS, where oxidative lipid damage was elevated [48]. The subsequent decline in MDA content may be attributed to the activity of antioxidant and detoxification enzymes, particularly glutathione S-transferase (GST), which plays a dual role in cellular defense [49,50]. GST facilitates the conjugation of glutathione (GSH) with electrophilic substrates to form more water soluble and less toxic derivatives, which are readily excreted or metabolized. GST also scavenges reactive oxygen species and lipid peroxidation products, thereby preserving membrane integrity [51]. As shown in Table 1, GST emerged as the dominant oxidative stress biomarker on day 35, indicating that prolonged PP exposure activated GST-mediated detoxification pathways. With extended stress duration, the toxicity of PP progressively intensified, leading to a collapse of the antioxidant defense system and extensive lipid peroxidation. In response, *Eisenia fetida* activated detoxifying enzymes like GST to counteract PP-induced toxicity [32]. Similar enzyme-mediated defense mechanisms have also been observed in studies investigating the effects of heavy metals on earthworms [45].

GPX is an important antioxidant enzyme that catalyzes the redox reaction between GSH and peroxides, such as H_2O_2 and superoxide radicals [52]. GPX activity has also been associated with the growth and reproductive capacity of earthworms [53]. As shown in Table 1, after 14 days of PLA exposure, GPX was identified as a sensitive oxidative stress biomarker, suggesting that the growth and reproduction of *Eisenia fetida* were affected during this period. This finding is consistent with the results of Shu et al. [53], who reported that short-term microplastic exposure could elevate GPX activity, thereby inhibiting growth and reproduction. On day 14, GPX had a factor loading value of 0.856, ranking second only to GST (loading = 0.994), indicating a strong response. However, as the stress duration increased, the correlation or "companion" relationship between GPX and GST diminished. This may be due to the antagonistic interaction between the two enzymes, as they compete for the common substrate GSH [54]. GPX activity is closely regulated by GSH availability, and only with sufficient GSH supplementation can GPX function optimally [55]. As shown in Figure 3, GPX activity increased again after 28 and 35 days of PLA exposure, suggesting a delayed but persistent oxidative response. Additionally, GPX helps protect the integrity and functionality of cell membranes from oxidative damage [56]. Interestingly, during this later stage, POD was identified as a key oxidative stress indicator, and TP content showed a strong negative loading (-0.997 for POD and -0.968 for TP), indicating a high level of peroxide accumulation and a decline in antioxidant capacity. These results suggest that both PLA and PP exposure caused significant damage to the antioxidant defense system and cell membrane integrity in earthworms. However, the mechanisms differed: PLA primarily triggered a POD-mediated response to peroxides, while PP induced a GST-dominant detoxification pathway.

AChE is a critical enzyme in neural signal transmission, responsible for degrading acetylcholine (ACh) to reduce neural excitation. AChE is widely regarded as one of the most effective biomarkers to evaluate neurotoxicity caused by environmental pollutants [57]. Elevated AChE activity can lead to acetylcholine depletion, impairing cholinergic signal transmission and adversely affecting cognition and memory [58]. In this study, AChE was identified as a sensitive oxidative stress biomarker from day 14 to day 35 under PS exposure (Table 1). However, Table A2 shows that as early as day 7, AChE exhibited a strong correlation with POD (factor loading = 0.927), and Figure 3 confirms a gradual increase in AChE activity beginning on day 14. These findings suggest that PS exposure triggered early-stage neurotoxicity in earthworms, which progressively intensified over time.

A similar response was observed under PLA exposure. At day 7, AChE exhibited a strong correlation with CAT (factor loading = 0.976), indicating early neural disruption. Previous studies also reported significant increases in AChE activity in earthworms exposed to PLA, with observable neurotoxic effects [59]. Compared to PP and PHA stress, PS and PLA induced earlier and more pronounced increases in AChE activity, suggesting that these microplastics may cause greater neurotoxicity during the early stages of exposure. The summary is shown in Figure 3. According to Tables A1 and A2, on day 21 of PHA exposure, AChE and MDA were identified as sensitive oxidative stress biomarkers, with factor loadings of 0.998 and 0.996, respectively. These results indicate that lipid peroxidation had occurred in earthworms, leading to cellular damage. The pronounced oxidative stress response reflected by elevated AChE activity may be attributed to lipid peroxidation in neural tissues, particularly the rupture of presynaptic vesicles containing neurotransmitters. This can result in an excessive accumulation of neurotransmitters in the synaptic cleft, subsequently stimulating increased AChE activity to degrade surplus acetylcholine [60]. Therefore, high AChE loadings of 0.900 and 0.871 were observed during days 28 to 35 under PHA stress, suggesting that PHA-induced neurotoxicity became more pronounced in the late stages of exposure (Figure 4).

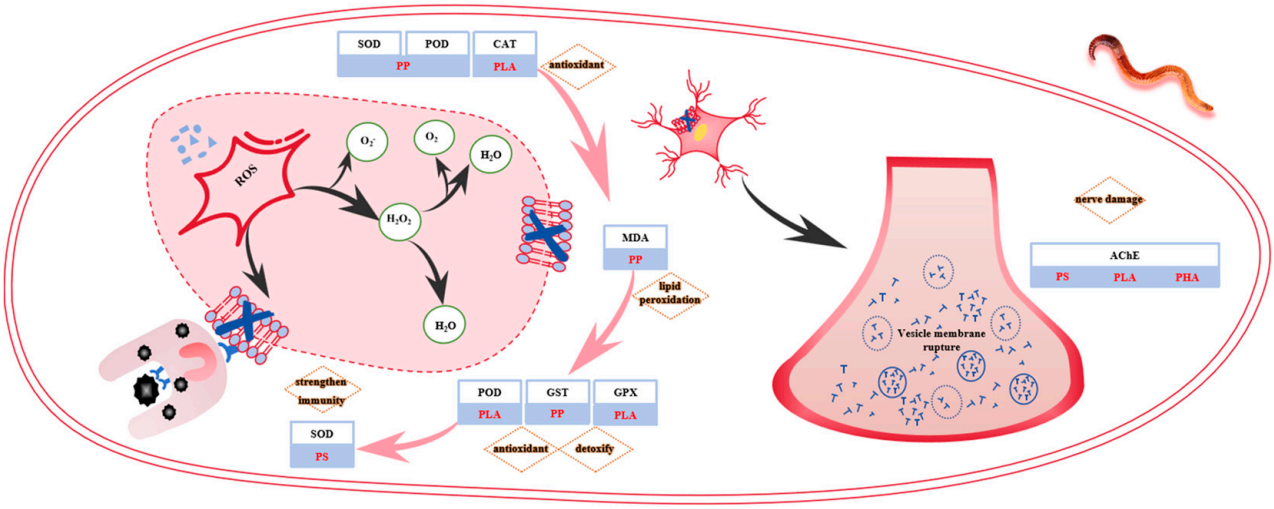


Figure 4. Mechanism diagram of the antioxidant system and nervous system of earthworms under microplastic stress.

Under PS exposure, SOD was identified as a sensitive oxidative stress indicator between days 21 and 28 (Table 1). However, Table A2 shows that TP content exhibited the highest negative loadings during this period, with values of −0.963 and −0.897, respectively. This may be closely related to the immune response of the earthworms. Previous studies by Yue et al. and Zhou et al. demonstrated that SOD plays a key role in enhancing phagocyte activity and systemic immune defense [14,61]. Thus, during this stress phase, metabolic dysfunction likely occurred in earthworms, with impaired protein synthesis and a shift in energy metabolism towards protein catabolism. In response, SOD activity increased to enhance immune function, maintain physiological homeostasis, and activate detoxification enzymes and neural regulation mechanisms. These coordinated responses help the organism recover from stress-induced damage. Similar physiological responses have been observed under cadmium exposure in earthworms [17].

3.3. Relationship Between the Physiological Response of Earthworms and Soil Ecological Functions Under Microplastic Stress

After standardizing the data S_{η}^{n}, an oxidative stress profile was constructed with microplastic concentration as the horizontal axis (Figure 5A). The results showed that oxidative stress responses varied across microplastic types and concentrations. Under exposure to conventional microplastics, PP exhibited a fluctuating trend of increase-decrease-increase, with the highest oxidative stress observed at 500 mg/kg. In contrast, PS followed a decrease–increase–decrease pattern, peaking at 100 mg/kg. In both cases, short-term exposure (7 and 14 days) resulted in higher oxidative stress levels than long-term exposure, suggesting that earthworms rapidly activated their antioxidant defense systems under low-concentration, short-term stress.

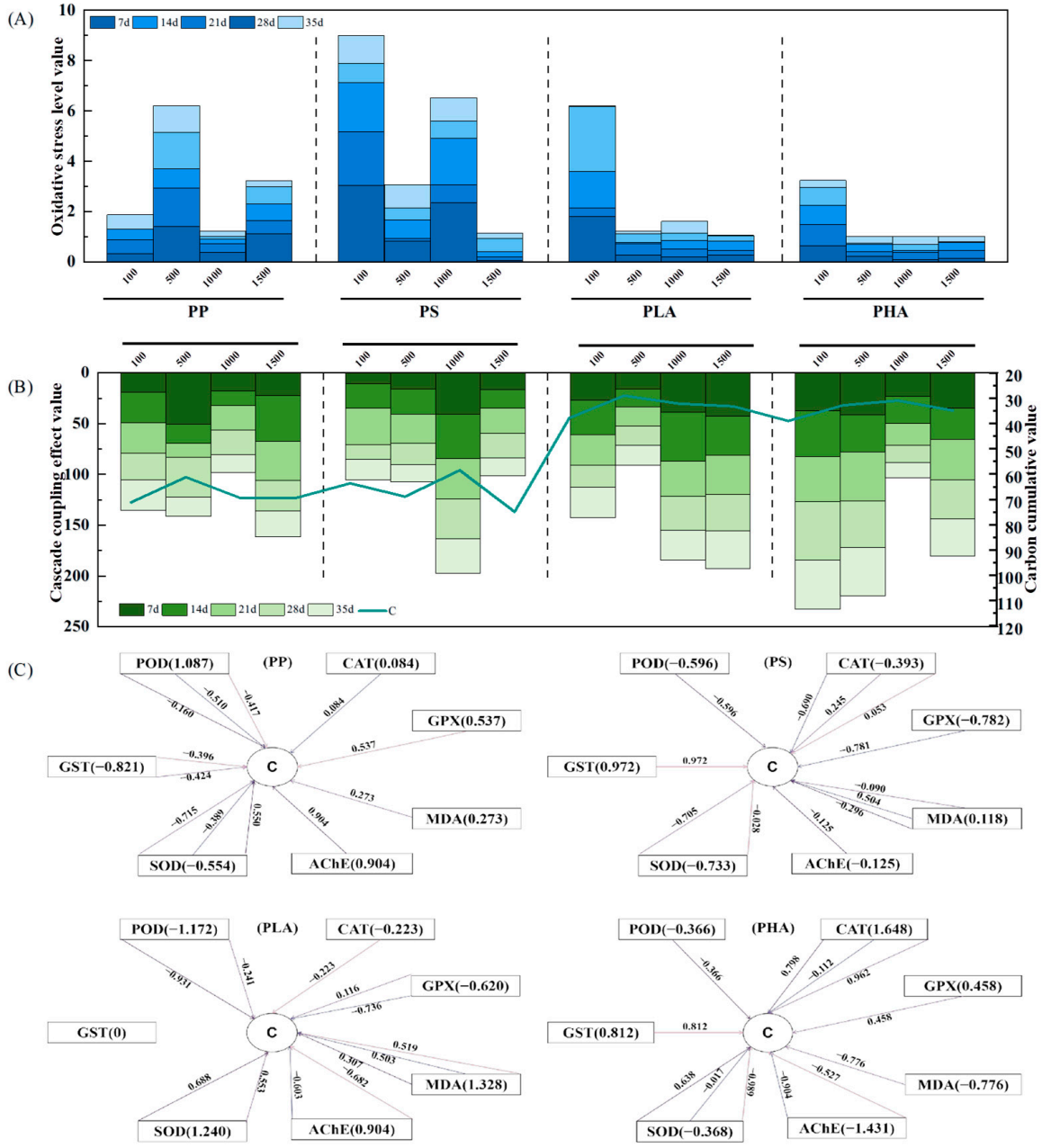


Figure 5. Toxicity of four types of microplastics on earthworms and soil ((**A**): the degree of oxidative stress in earthworms; (**B**): cascade coupling effect diagram; (**C**): correlation coefficient graph of earthworm oxidative stress indicators and soil total).

However, with prolonged exposure and increased concentrations, oxidative stress levels gradually declined, indicating potential suppression or exhaustion of the antioxidant defense system, which may result in oxidative damage. This reduction in defense capacity could be linked to the accumulation of microplastics in the gastrointestinal tract, leading to intestinal injury, shifts in gut microbiota, and subsequent disruption of antioxidant functions [21]. Similar findings have been reported in earthworms exposed to polyethylene microplastics (250–1000 μm) and polystyrene microplastics (5 μm and 20 μm), which induced oxidative stress and physiological disruption [19,62]. Under biodegradable microplastic exposure (PLA and PHA), oxidative stress patterns were relatively similar. Both exhibited the highest stress response at 100 mg/kg, with minimal changes in oxidative stress levels across increasing concentrations. This indicates that exposure to PLA in soil can inhibit the growth of earthworms, lead to a decrease in earthworm biomass [63], and also trigger oxidative stress in the body, causing DNA damage [64].

Based on the changes in total soil carbon under different microplastic stresses shown in Figure 5B, it can be concluded that under traditional microplastic stress, the content of total soil carbon is relatively high. This may be due to the fact that soil structure (e.g., porosity and aggregate stability) is a key factor determining soil carbon sequestration capacity [65]. The decomposition process of microplastics indirectly regulates the stability of organic matter by altering soil structure [66]. Previous studies have confirmed that traditional microplastics (e.g., PE and PVC) can increase the proportion of small-particle aggregates in soil. These small-particle aggregates mainly immobilize organic carbon through chemical reactions, which significantly reduces the decomposition rate of organic carbon and thus is more conducive to long-term soil carbon sequestration [67]. At the same time, the hydrophobicity of PP and PS particles can reduce the hydraulic conductivity of soil capillary pores, decrease the loss of organic matter via water leaching, and further promote the accumulation of soil organic matter [68].

The decomposition of biodegradable microplastics (e.g., PLA and PHA) exerts a "dynamic impact" on soil structure. In the initial stage, similar to traditional microplastics, biodegradable microplastics promote the formation of small-particle aggregates. However, as their degradation progresses, these biodegradable microplastics continue to release soluble organic matter, which further binds soil particles and gradually forms large-particle aggregates [69]. The carbon immobilization by large-particle aggregates mainly relies on physical encapsulation, and their turnover rate is relatively fast. Compared with the chemically stable carbon immobilization by small-particle aggregates, their long-term carbon sequestration capacity is weaker [70]. Another study has confirmed that adding polyester (PET) ultrafine fibers (a type of non-biodegradable microplastics) to soil significantly reduces soil bulk density and the number of water-stable aggregates, further reflecting the potential damage of such non-biodegradable microplastics to soil structure [71]. In addition, earthworm activity accelerates the degradation process of biodegradable microplastics and promotes their release of more soluble organic matter, and these soluble organic compounds are more prone to leaching and loss with soil water, ultimately leading to a decrease in total soil carbon content [72].

Similarly to traditional microplastics, the antioxidant defense system of earthworms can effectively mitigate oxidative stress at low concentrations. However, as the concentration increases and surpasses the antioxidant threshold, this defense system becomes overwhelmed and ultimately fails [73]. Among the four types of microplastics tested, PS exhibited the highest toxicity. This may be attributed to the rapid formation of a protein corona, a layer of adsorbed proteins on the PS surface upon contact with biological systems, which enhances its biological reactivity and toxicity [74]. Moreover, the relatively high surface charge and polarity of PS particles may increase their affinity for cell membranes and

biomolecules, facilitating cellular uptake and prolonging retention time in organisms [75]. These interactions can stimulate ROS production, disrupt membrane integrity, and promote lipid peroxidation [76].

Degradable microplastics can undergo hydrolysis or biodegradation in soil to form soluble organic substances such as oligomers or monomers [77], thereby increasing soil organic carbon. And the increase in biodegradable microplastics is significantly greater than that of traditional non-biodegradable microplastics [78]. However, in this study, as shown in Figure 5B, the soil organic matter content in the PP and PS stress groups was significantly higher than that in the PLA and PHA stress groups. However, the cascading coupling effect value was significantly higher in the PLA and PHA stress groups than in the PP and PS stress groups. On the one hand, this may be due to the "substrate competition" between the degradation process of biodegradable microplastics and the organic matter mineralization process mediated by earthworms, which amplifies the "obstacles" to both parties. Due to the release of a large amount of carbon sources that are easily utilized by microorganisms during the degradation process of biodegradable plastics, their changes in microbial community turnover and structure are stronger than those of traditional plastics [79,80], leading to the gradual succession of microbial communities to predominantly eutrophic microorganisms (r strategy) [81]. As a typical countermeasure organism, earthworms compete with soil microbial communities for high-energy and easily utilizable substrates, especially when resources are limited or external stress occurs.

On the other hand, it may be caused by the toxic effects of additives in plastic products. Although the ultimate goal of biodegradable microplastics is to mineralize plastic products into carbon dioxide and water, commercially produced PLA and PHA plastic products typically contain additives (such as plasticizers, nucleating agents, masterbatch, and antioxidants) that gradually release into the surrounding environment as the plastic degrades. Biodegradable microplastics can affect the physiological and biochemical processes of organisms, causing growth inhibition, oxidative stress, and inducing cell damage [82]. In this study (Appendix C), the path analysis model showed that the remaining path coefficients were all less than 0.25, and the model validation passed. This indicates that there is a close cascade coupling effect between oxidative stress indicators in earthworms and soil total carbon content after the occurrence of microplastic stress. Further research found (Figure 5C) that the highest cumulative pathway effect coefficient of the PLA stress group was 1.328, while the PHA stress group could reach 1.648. Both were much higher than the PP and PS stress groups (the former was 0.904; the latter was 0.971). This also confirms that biodegradable microplastics are not friendly to soil ecosystems. In the future, it is necessary to further evaluate their ecological toxicity and focus on studying the aging, degradation, release of intermediate products and additives of biodegradable microplastics in soil.

4. Conclusions

This study is the first to integrate the oxidative stress effect of microplastics on *Eisenia fetida* with the competition between the degradation of biodegradable microplastics and earthworm-mediated organic mineralization for substrates, and construct a joint pathway analysis model of biological physiological responses and soil ecological functions. This model realizes the cross-scale correlation between individual physiological toxicity and ecosystem function, providing a new framework for quantifying the comprehensive harm of microplastics and filling the gap in the physiological–ecological linkage in the ecological safety assessment of degradable plastics.

The stage pattern of oxidative stress markers, SOD, POD, and CAT, are warning markers in the early stage (day 7); POD, GST, and GPX dominate free radical scavenging and cell repair in the middle stage; and SOD activates the immune–detoxification–neural

synergistic mechanism to cope with long-term stress in later stages, providing a basis for temporal dynamic assessment. The toxicity mechanism of different microplastic types, PLA, PHA, PP, and PS, all cause significant damage to the antioxidant defense system and cell membrane integrity of earthworms, but PLA relies on POD to clear peroxides and PP relies on GST for detoxification. PLA- and PS-induced nerve damage occurs in the early stages of exposure, while the neurotoxic effects of PHA manifest in later stages of stress. This thus provides key evidence revealing the long-term risks of biodegradable plastics. Risk confirmation of biodegradable microplastics: although PLA and PHA are biodegradable, they inhibit earthworm-mediated organic mineralization through substrate competition and cause oxidative stress and nerve damage, confirming that they are not environmentally friendly, especially in soil ecosystems.

In summary, these findings provide new insights into the different toxicity mechanisms of traditional and biodegradable microplastics, and provide a scientific basis to evaluate the ecological risks of microplastic pollution in soil and whether biodegradable plastics are truly environmentally friendly.

Author Contributions: Conceptualization, Y.N.; methodology, Y.L., D.Z. and Y.N.; software, D.Z. and H.W.; validation, Y.L., D.Z. and W.Z.; formal analysis, Y.L.; investigation, Y.L., H.W., W.Z. and R.W.; resources, Y.N.; data curation, Y.L., H.W., W.Z. and R.W.; writing—original draft preparation, Y.L.; writing—review and editing, D.Z. and Y.N.; visualization, H.W.; supervision, Y.N.; project administration, Y.N.; funding acquisition, D.Z. and Y.N. All authors have read and agreed to the published version of this manuscript.

Funding: This research was funded by the National Natural Science Foundation of China (42107327), the Heilongjiang Provincial Natural Science Foundation (YQ2021D002), and the Science and Technology Department of Heilongjiang Province (2022ZXJ08B01-1).

Institutional Review Board Statement: Not applicable.

Informed Consent Statement: Not applicable.

Data Availability Statement: The sequencing data have been uploaded to the Science Data Bank. If readers need to the data, they can click on the link: https://www.scidb.cn/s/ZBVfmm (accessed on 7 March 2025).

Acknowledgments: Thank you to the Mathematical Modeling Teaching and Research Office of Northeast Agricultural University for their assistance in data analysis, especially Zhang Zhanguo for meticulous guidance and assistance in using mathematical modeling to analyze and synthesize research data.

Conflicts of Interest: The authors declare no conflicts of interest.

Abbreviations

The following abbreviations are used in this manuscript:

PP	polypropylene
PS	polystyrene
PLA	polylactic acid
PHA	polyhydroxyalkanoates
TP	total protein
POD	peroxidase
SOD	superoxide dismutase
GPX	glutathione peroxidase
GST	glutathione-S-transferase
CAT	catalase
MDA	malondialdehyde

TBA	thiobarbituric acid
AChE	acetylcholinesterase

Appendix A

Z-Score Method for Standardization

Standardization of data. In this study, the Z-score method was used to standardize the original data, calculated as: $x_{pq}{}' = \frac{x_{pq}-\overline{x}_q}{S_q}$, where $p = 1,2,\cdots,j$; $q = 1,2,\cdots,n$; $\overline{x}_q = \frac{1}{j}\sum_{p=1}^{j} x_{pq}$; $S_Q^2 = \frac{1}{j-1}\sum_{p=1}^{j}\left(x_{pq}-\overline{x}_q\right)^2$

Next, the correlation coefficient matrix of the sample matrix is computed as:

$$R = \begin{Bmatrix} r_{11} & r_{12} & \cdots & r_{1n} \\ r_{21} & r_{22} & \cdots & r_{2n} \\ \cdots & \cdots & \cdots & \cdots \\ r_{n1} & r_{n2} & \ldots & r_{nm} \end{Bmatrix}$$

To perform principal component extraction, the eigenvectors and eigenvalues of the correlation matrix *R* are calculated. The Jacobi method is used to solve the characteristic equation: $|R-\lambda I| = 0$, $\lambda_1 > \lambda_2 > \cdots \lambda_n \geq 0$. The corresponding eigenvectors for each eigenvalue λ_φ are:

$$C^{(q)} = \left\{C_1^{(q)}, C_2^{(q)}, \cdots, C_n^{(q)}\right\}, q = 1,2,\cdots,n$$

These eigenvectors satisfy the orthogonality condition: $C^{(q)}C^{(k)} = \sum_{p=1}^{n} C_p^{(q)}C_p^{(k)} = \begin{cases} 1 & (q=k) \\ 0 & q \neq k \end{cases}$

Selection of the principal component. When the variance of the first *m* principal components $P_1, P_2, \cdots, P_m (m < n)$ and the proportion *a* of the total variance meet the following conditions, the first *m* components $P_1, P_2, \cdots, P_m (m < n)$ are selected as 1, 2, …, *m* principal components.

$$\alpha = \frac{\sum_{\varphi=1}^{m}\lambda_\varphi}{\sum_{\varphi=1}^{n}\lambda_\varphi} \geq 0.85$$

To perform statistical analysis, the score of each principal component $C_{\eta j}$ and the comprehensive score of each sample S_η were calculated using the following formulas: The number of principal components $\eta = 1,2,\ldots,m$; the number of oxidative stress indicators of microplastic $j = 1,2,\ldots,7$; stress concentration $n = 12\ldots9$.

$$C_{\eta=1}^{n} = \varepsilon_{\eta 1}X_{j1} + \varepsilon_{\eta 2}X_{j2} + \cdots + \varepsilon_{\eta n}X_{jn}\ , S_{\eta=1}^{n} = \left|\sum_{\eta=1}^{m} C_{\eta j}^{n}\xi_\eta\right|$$

Appendix B

Extraction and Interpretation of the Main Factors

Taking an eigenvalue greater than 1 as the extraction standard, the number of the main factors under different micro plastic stress was obtained. The cumulative contribution rates of the main factors extracted were 82.259–100.000%, except for the treatment of PLA exposure for the 35th day, which was 76.798%. Among them, the contribution rate of the 14th day under PP and PLA stress, the 21st day under PP stress, and the 28th day under PS stress was more than 95%, and the cumulative contribution rate of variance after rotation did not change, indicating that the common factors extracted by each group can represent most of the information in the original data.

Table A1. Eigenvalue, contribution rate and cumulative contribution rate of the main factors.

Principal Factor	Sum of Extracted Square Loads			Sum of Rotating Square Loads		
	Eigen Value	Contribution Rate%	Cumulative Contribution Rate%	Eigen Value	Contribution Rate%	Cumulative Contribution Rate%
Fpp-7-1	5.424	67.803	67.803	5.282	66.022	66.022
Fpp-7-2	1.773	22.167	89.97	1.916	23.948	89.97
Fps-7-1	5.772	72.147	72.147	4.399	54.989	54.989
Fps-7-2	1.754	21.92	94.067	3.126	39.078	94.067
Fpla-7-1	7.07	88.371	88.371	-	-	-
Fpha-7-1	6.356	79.455	79.455	4.522	56.521	56.521
Fpha-7-2	1.178	14.731	94.186	3.013	37.665	94.186
Fpp-14-1	5.018	62.723	62.723	5.004	62.55	62.55
Fpp-14-2	1.682	21.022	83.745	1.383	17.292	79.841
Fpp-14-3	1.019	12.733	96.478	1.331	16.636	96.478
Fps-14-1	4.276	53.456	53.456	3.641	45.508	45.508
Fps-14-2	1.823	22.784	76.24	1.997	24.961	70.469
Fps-14-3	1.387	17.338	93.577	1.849	23.109	93.577
Fpla-14-1	3.705	46.307	46.307	3.091	38.638	38.638
Fpla-14-2	2.894	36.176	82.483	2.999	37.491	76.129
Fpla-14-3	1.327	16.591	99.074	1.836	22.945	99.074
Fpha-14-1	4.403	55.039	55.039	3.667	45.84	45.84
Fpha-14-2	2.4	30.005	85.044	3.136	39.204	85.044
Fpp-21-1	4.662	58.274	58.274	3.55	44.37	44.37
Fpp-21-2	1.772	22.149	80.423	2.516	31.449	75.819
Fpp-21-3	1.413	17.657	98.08	1.781	22.261	98.08
Fps-21-1	6.586	82.321	82.321	-	-	-
Fpla-21-1	6.796	84.951	84.951	-	-	-
Fpha-21-1	7.261	90.765	90.765	-	-	-
Fpp-28-1	3.148	39.348	39.348	2.845	35.566	35.566
Fpp-28-2	2.446	30.574	69.922	2.666	33.328	68.895
Fpp-28-3	1.95	24.38	94.302	2.033	25.408	94.302
Fps-28-1	3.894	48.67	48.67	3.71	46.379	46.379
Fps-28-2	2.283	28.536	77.206	2.396	29.95	76.329
Fps-28-3	1.611	20.141	97.347	1.681	21.018	97.347
Fpla-28-1	5.164	64.546	64.546	4.521	56.517	56.517
Fpla-28-2	2.224	27.805	92.351	2.867	35.834	92.351
Fpha-28-1	5.018	62.729	62.729	3.588	44.853	44.853
Fpha-28-2	1.562	19.53	82.259	2.993	37.407	82.259
Fpp-35-1	4.091	51.132	51.132	3.682	46.03	46.03
Fpp-35-2	1.795	22.433	73.565	2.009	25.113	71.143
Fpp-35-3	1.533	19.163	92.728	1.727	21.585	92.728
Fps-35-1	4.254	53.176	53.176	3.818	47.725	47.725
Fps-35-2	2.612	32.654	85.83	3.048	38.105	85.83
Fpla-35-1	4.138	51.719	51.719	3.336	41.704	41.704
Fpla-35-2	1.892	23.654	75.373	2.64	33	74.704
Fpla-35-3	1.328	16.602	91.974	1.382	17.27	91.974
Fpha-35-1	4.628	57.856	57.856	4.393	54.908	54.908
Fpha-35-2	1.515	18.943	76.798	1.751	21.891	76.798

Notes: Fa-b-c represents the C major factor of PP, PS, PLA and PHA microplastics stress on the B day.

Appendix C

Analysis of Factor Load Matrix

In order to solve practical problems, we should not only extract the main factors, but also understand the practical significance of each factor. Therefore, it is necessary to rotate the factor load matrix to better explain the practical significance of each factor. In this study, the maximum variance method is used to rotate the load matrix of the original factor orthogonally, and SPSS 19.0 is used to calculate the factor load matrix after rotation, so as to ensure that each factor can be interpreted more accurately. This indicates the main factor load of eight indicators (TP, POD, CAR, MDA, SOD, AchE, GST, and GPX) on that day, and reflects the correlation between the main factor and the original data.

The common degree indicates the degree to which the information contained in each variable can be interpreted by the extracted principal components. The closer the value is to 1, the better. In all treatment groups, the commonality reached the highest of 1, most of which was greater than 0.8, indicating that most of the information of variables can be explained by the main factor, and the information of variables is less lost, and the overall effect of factor extraction is ideal. On the 21st day of PLA stress, the commonality of POD, CAT, MDA and AchE was greater than 0.9, that of SOD and GPX was greater than 0.8, and that of GST was 0.393, which was the smallest among all the experimental groups, indicating that the information of POD, SOD, CAT, MDA, AchE and GPX were retained relatively completely and the extraction effect was ideal.

Taking the 7th day under PP stress as an example to explain the significance of each main factor, Fpp-7-1 (the first main factor), the eigenvalue was 5.424, the contribution rate was 67.803%, and the contribution rate after rotation was 66.022%. The main correlation indexes are SOD and GPX, which are highly correlated. The maximum factor load in the positive axis direction is SOD (the factor load after rotation is 0.983), and the maximum factor load in the negative axis direction is GPX (the factor load after rotation is −0.98). The load of the two indexes in the first main factor is greater than 0.98, and is more closely related to the first main factor fpp-1-1.

Table A2. Factor load matrix and common degree of variables.

Principal Factor	Feature Vector							
	TP	**POD**	**CAT**	**MDA**	**SOD**	**AChE**	**GST**	**GPX**
Fpp-7-1	−0.919	0.277	0.934	0.975	0.983	0.738	0.255	−0.98
Fpp-7-2	−0.357	−0.756	−0.287	0.036	0.183	0.642	0.828	0.044
Communalities	0.972	0.649	0.956	0.952	1	0.956	0.751	0.963
Fps-7-1	−0.724	0.957	0.184	0.766	0.769	0.927	0.062	0.941
Fps-7-2	−0.676	0.273	0.909	0.576	0.578	0.327	0.959	−0.277
Communalities	0.788	0.995	0.985	0.929	0.976	0.945	0.907	0.962
Fpla-7-1	−0.986	0.941	0.998	0.955	0.968	0.976	0.925	−0.749
Communalities	0.971	0.886	0.996	0.912	0.936	0.952	0.856	0.561
Fpha-7-1	−0.814	0.97	0.817	0.916	0.919	0.503	0.558	−0.059
Fpha-7-2	−0.558	0.027	0.553	0.376	0.379	0.686	0.806	−0.996
Communalities	0.974	0.942	0.973	0.98	0.987	0.724	0.96	0.995

Table A2. *Cont.*

Principal Factor	Feature Vector							
	TP	**POD**	**CAT**	**MDA**	**SOD**	**AChE**	**GST**	**GPX**
Fpp-14-1	−0.987	0.862	0.159	0.966	0.955	0.927	0.088	0.74
Fpp-14-2	−0.139	−0.385	0.954	0.237	0.016	0.312	−0.179	−0.345
Fpp-14-3	−0.059	0.324	−0.148	−0.032	0.152	−0.204	0.954	−0.475
Communalities	0.997	0.997	0.958	0.991	0.935	0.998	0.949	0.893
Fps-14-1	0.506	−0.731	0.855	0.104	−0.945	0.96	0.224	−0.491
Fps-14-2	−0.698	0.574	−0.431	0.957	0.088	0.144	0.225	−0.025
Fps-14-3	−0.213	0.361	0.261	0.053	0.273	0.046	0.898	0.849
Communalities	0.788	0.995	0.985	0.929	0.976	0.945	0.907	0.962
Fpla-14-1	0.351	−0.044	−0.084	0.252	−0.659	−0.861	0.856	0.994
Fpla-14-2	−0.933	0.067	0.98	0.938	−0.253	0.466	−0.014	0.038
Fpla-14-3	0.047	0.993	−0.169	0.201	0.703	0.113	−0.516	0.062
Communalities	0.996	0.993	0.995	0.984	0.993	0.971	0.999	0.993
Fpha-14-1	−0.073	0.971	0.136	0.636	0.816	−0.179	−0.967	0.814
Fpha-14-2	−0.973	0.23	0.944	0.772	0.508	0.588	0.111	−0.183
Communalities	0.953	0.996	0.91	1	0.924	0.378	0.947	0.696
Fpp-21-1	−0.884	0.929	0.923	0.328	0.142	0.903	−0.025	0.331
Fpp-21-2	−0.466	0.319	−0.061	0.927	−0.217	0.349	0.62	0.883
Fpp-21-3	−0.03	0.098	0.332	0.138	0.947	−0.247	0.777	−0.279
Communalities	1	0.974	0.966	0.987	0.965	0.997	0.989	0.968
Fps-21-1	−0.963	0.839	0.821	0.949	0.953	0.938	0.941	0.84
Communalities	0.928	0.704	0.674	0.901	0.908	0.879	0.886	0.705
Fpla-21-1	−0.971	0.991	0.954	0.985	0.909	0.952	0.627	0.93
Communalities	0.944	0.982	0.911	0.97	0.827	0.906	0.393	0.864
Fpha-21-1	−0.976	0.992	0.98	0.996	0.93	0.998	0.794	0.938
Communalities	0.952	0.984	0.961	0.993	0.864	0.997	0.631	0.88
Fpp-28-1	−0.455	0.932	0.854	0.932	0.16	−0.36	−0.072	−0.113
Fpp-28-2	−0.878	0.223	0.013	−0.068	0.974	0.914	0.203	0.128
Fpp-28-3	−0.117	0.049	0.378	−0.348	−0.159	0.186	0.934	−0.905
Communalities	0.991	0.92	0.872	0.993	1	0.999	0.92	0.849
Fps-28-1	−0.897	0.317	0.919	−0.609	0.988	0.082	0.223	0.746
Fps-28-2	−0.37	0.915	0.36	0.219	0.054	0.955	−0.03	−0.573
Fps-28-3	−0.176	0.247	−0.052	0.761	−0.078	−0.057	0.973	0.226
Communalities	0.972	0.999	0.978	0.998	0.985	0.922	0.998	0.936
Fpla-28-1	−0.997	0.896	0.246	0.83	0.572	0.858	−0.354	0.887
Fpla-28-2	−0.032	0.4	0.91	−0.332	−0.72	−0.497	0.894	−0.449
Communalities	0.995	0.962	0.889	0.799	0.846	0.983	0.925	0.988
Fpha-28-1	−0.859	0.462	−0.183	0.693	0.392	0.9	−0.8	0.721
Fpha-28-2	−0.27	0.787	0.895	0.475	0.891	0.21	0.086	0.654
Communalities	0.81	0.834	0.834	0.705	0.947	0.854	0.647	0.948
Fpp-35-1	−0.114	−0.335	0.896	0.906	−0.409	−0.881	0.991	−0.096
Fpp-35-2	0.157	0.773	0.335	−0.194	0.343	0.379	−0.113	−0.982
Fpp-35-3	0.969	−0.293	0.105	0.376	−0.72	0.032	−0.061	−0.163
Communalities	0.977	0.795	0.925	1	0.803	0.921	0.999	1
Fps-35-1	0.541	−0.908	0.6	0.797	0.072	0.949	−0.461	−0.767
Fps-35-2	−0.781	−0.274	0.785	0.124	0.952	0.237	−0.771	0.418
Communalities	0.902	0.9	0.976	0.65	0.911	0.957	0.807	0.763
Fpla-35-1	−0.968	0.898	0.129	0.361	0.746	0.304	−0.247	0.858
Fpla-35-2	0.046	0.004	−0.901	0.453	0.643	0.558	−0.919	0.229
Fpla-35-3	0.105	0.329	−0.058	0.798	0.132	−0.771	0.05	−0.086

Table A2. *Cont.*

Principal Factor	Feature Vector							
	TP	POD	CAT	MDA	SOD	AChE	GST	GPX
Communalities	0.95	0.915	0.831	0.972	0.987	0.998	0.909	0.796
Fpha-35-1	−0.899	0.744	0.6	0.822	0.885	0.871	−0.042	0.673
Fpha-35-2	−0.378	0.534	0.215	−0.077	0.449	−0.344	0.974	−0.054
Communalities	0.951	0.838	0.406	0.681	0.985	0.876	0.95	0.456

Appendix D

Principal Component Comprehensive Score Chart

Based on the PCA model, linear regression equations for the principal components of each experimental group were established. Using the variance contribution rate of each principal component as a weighting factor, the scores of principal components ($C^n_{\eta j}$, summarized in Figure 5) and comprehensive evaluation scores (S^n_η, summarized in Table A2) were calculated for the treatment groups at different exposure durations.

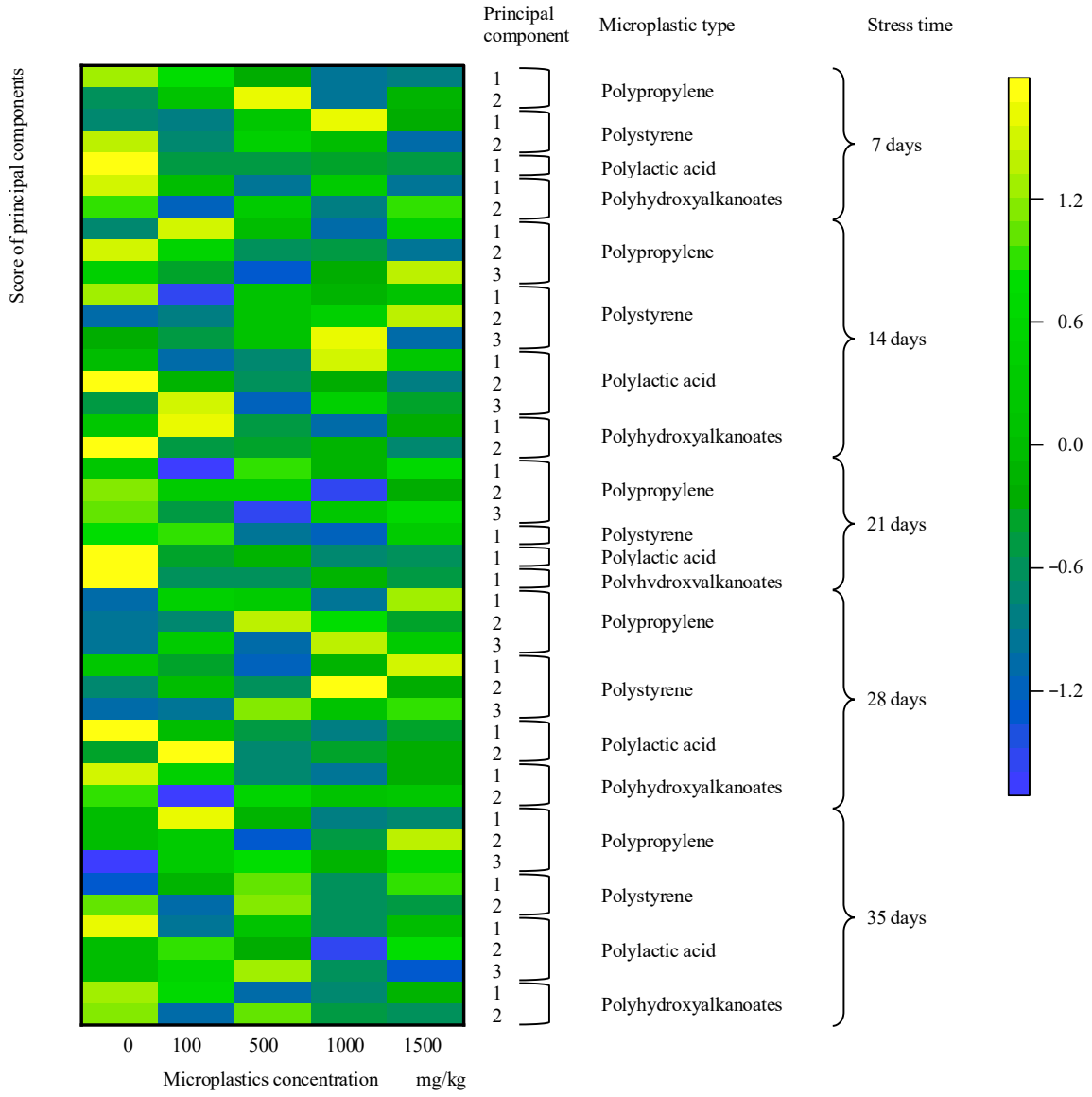


Figure A1. Principal component comprehensive score chart.

Appendix E

Partial Results of Path Analysis

Table A3. Summary of path analysis model.

Stress Concentration (PP)	Factor	Direct Path Coefficient	Indirect Path Coefficient			Coefficient of Determination	Total Indirect Coefficient	Total Effect
				PP				
			→X1	→X5	→X6			
100 mg/kg	X1	−0.894		0.392	0.086	0.947	0.478	0.417
	X5	−0.749	0.468		−0.116		0.352	0.396
	X6	0.517	−0.148	0.168			0.020	0.537
			→X3	→X5	→X7			
500 mg/kg	X3	−1.248		0.103	0.431	0.971	0.534	0.715
	X5	0.519	−0.247		−0.696		−0.943	0.424
	X7	1.094	−0.492	−0.330			−0.821	0.273
			→X1	→X2	→X3			
1000 mg/kg	X1	−2.104		1.167	0.427	0.994	1.594	0.510
	X2	1.467	−1.674		0.291		−1.383	0.084
	X3	0.519	−1.731	0.823			−0.908	0.389
			→X1	→X3	→X4			
1500 mg/kg	X1	−0.403		−0.054	0.297	0.999	0.242	0.160
	X3	−0.184	−0.119		0.852		0.733	0.550
	X4	1.145	−0.104	−0.137			−0.241	0.904
				PS				
			→X2	→X3	→X5			
100 mg/kg	X2	−0.277		0.414	−0.084	0.998	0.330	0.053
	X3	0.463	−0.248		−0.243		−0.491	0.028
	X5	1.056	0.022	−0.107			−0.085	0.971
			→X2	→X3	→X7			
500 mg/kg	X2	1.279		−0.391	−0.643	0.980	−1.035	0.245
	X3	−0.986	0.508		−0.262		0.246	0.741
	X7	0.708	−1.162	0.365			−0.798	0.090
			→X2	→X6	→X7			
1000 mg/kg	X2	−1.175		0.254	0.231	0.999	0.485	0.690
	X6	0.335	−0.891		−0.224		−1.115	0.781
	X7	0.892	−0.304	−0.084			−0.388	0.504
			→X1	→X4	→X7			
1500 mg/kg	X1	−2.255		1.335	0.324	0.988	1.659	0.596
	X4	1.586	−1.898		0.187		−1.711	0.125
	X7	0.528	−1.385	0.560			−0.824	0.296
				PLA				
			→X2	→X4	→X7			
100 mg/kg	X2	2.041		0.010	−2.274	0.980	−2.264	0.223
	X4	−0.273	−0.072		−0.339		−0.411	0.683
	X7	2.408	−1.928	0.038			−1.889	0.519
			→X1	→X3	→X6			
500 mg/kg	X1	−0.992		−0.538	1.289	0.988	0.751	0.241
	X3	1.027	0.520		−0.994		−0.475	0.553
	X6	1.576	−0.812	−0.648			−1.460	0.116
			→X4	→X6	→X7			
1000 mg/kg	X4	0.088		−0.574	−0.117	0.999	−0.691	0.603
	X6	−0.941	0.054		0.151		0.205	0.736
	X7	0.716	−0.014	−0.199			−0.213	0.503
			→X1	→X3	→X7			
1500 mg/kg	X1	−0.751		−0.156	−0.025	0.998	−0.181	0.931
	X3	0.339	0.346		0.004		0.349	0.688
	X7	0.215	0.086	0.006			0.092	0.307
				PHA				
			→X3	→X4	→X5			
100 mg/kg	X3	−0.845		−0.061	−0.083	0.998	−0.144	0.989
	X4	−0.147	−0.349		−0.031		−0.380	0.527
	X5	0.105	0.664	0.043			0.707	0.812
			→X2	→X6	→X7			
500 mg/kg	X2	0.944		−0.123	0.141	0.999	0.018	0.962
	X6	−0.191	0.609		0.041		0.649	0.458
	X7	−0.230	−0.579	0.034			−0.546	0.776

Table A3. *Cont.*

Stress Concentration (PP)	Factor	Direct Path Coefficient	Indirect Path Coefficient			Coefficient of Determination	Total Indirect Coefficient	Total Effect
			→X2	→X3	→X4			
1000 mg/kg	X2	0.166		−0.212	−0.067	0.958	−0.278	0.112
	X3	−0.459	0.077		0.366		0.442	0.017
	X4	−1.071	0.010	0.157			0.167	0.904
			→X1	→X2	→X3			
1500 mg/kg	X1	−0.065		−0.221	−0.079	1.000	−0.300	0.366
	X2	0.750	0.019		0.029		0.049	0.798
	X3	0.592	0.009	0.037			0.046	0.638

→*a*: Indirect path effect through indicator *a*.

References

1. Li, S.H.; Li, Y.Z.; An, H.X.; Lian, J. Research status and hot trends of microplastics in the soil environment based on bibliometric methods. *China Coal Chem. Ind.* **2024**, *47*, 149–154.
2. Thompson, R.C.; Olsen, Y.; Mitchell, R.P.; Davis, A.; Rowland, S.J.; John, A.W.; Mcgonigle, D.; Russell, A.E. Lost at sea: Where is all the plastic? *Science* **2004**, *304*, 838. [CrossRef]
3. Zhang, Y.; Dou, M.; Hao, S.Z.; Li, P.; Wang, G.H.; Zhou, Y.Z.; Liang, Z.J. Research progress and prospects on the occurrence characteristics of microplastics in farmland soils in China. *J. Irrig. Drain.* **2024**, *43*, 11–20.
4. Steinmetz, Z.; Wollmann, C.; Schaefer, M.; Buchmann, C.; David, J.; Tröger, J.; Muñoz, K.; Frör, O.; Schaumann, G.E. Plastic mulching in agriculture. Trading short-term agronomic benefits for long-term soil degradation? *Sci. Total Environ.* **2016**, *550*, 690–705. [CrossRef] [PubMed]
5. Auta, H.S.; Emenike, C.U.; Fauziah, S.H. Distribution and importance of microplastics in the marine environment: A review of the sources, fate, effects, and potential solutions. *Environ. Int.* **2017**, *102*, 165–176. [CrossRef] [PubMed]
6. United Nations Environment Programme. "Zero Draft of the Plastics Treaty (UNEP/PP/INC.3/4)". 2023. Available online: https://wedocs.unep.org/bitstream/handle/20.500.11822/43239/ZERODRAFT.pdf (accessed on 12 August 2025).
7. European Bioplastics. "Bioplastic Market Development Update 2024". 2024. Available online: https://www.european-bioplastics.org/bioplastics-market-development-update-2024/ (accessed on 12 August 2025).
8. Karan, H.; Funk, C.; Grabert, M.; Oey, M.; Hankamer, B. Green bioplastics as part of a circular bioeconomy. *Trends Plant Sci.* **2019**, *24*, 237–249. [CrossRef]
9. European Parliament and Council. "Directive (EU) 2019/904 of the European Parliament and of the Council of 5 June 2019 on the Reduction of the Impact of Certain Plastic Products on the Environment. 2019. Available online: http://data.europa.eu/eli/dir/2019/904/oj (accessed on 12 August 2025).
10. Blouin, M.; Hodson, M.E.; Delgado, E.A.; Baker, G.; Brussaard, L.; Butt, K.R.; Dai, J.; Dendooven, L.; Peres, G.; Tondoh, J.E.; et al. A review of earthworm impact on soil function and ecosystem services. *Eur. J. Soil Sci.* **2013**, *64*, 161–182. [CrossRef]
11. Plaas, E.; Meyer-Wolfarth, F.; Banse, M.; Bengtsson, J.; Bergmann, H.; Faber, J.; Potthoff, M.; Runge, T.; Schrader, S.; Taylor, A. Towards valuation of biodiversity in agricultural soils: A case for earthworms. *Ecol. Econ.* **2019**, *159*, 291–300. [CrossRef]
12. Calisi, A.; Zaccarelli, N.; Lionetto, M.G.; Schettino, T. Integrated biomarker analysis in the earthworm Lumbricus terrestris: Application to the monitoring of soil heavy metal pollution. *Chemosphere* **2013**, *90*, 2637–2644. [CrossRef]
13. Forman, E.; Gass, S. The Analytic Hierarchy Process—An Exposition. *Oper. Res.* **2001**, *49*, 468–486. [CrossRef]
14. Zhou, D.X.; Ning, Y.C.; Jin, C.M.; Liu, L.Y.; Pan, X.L.; Cao, X. Correlation of the oxidative stress indices and Cd exposure using a mathematical model in the earthworm, *Eisenia fetida*. *Chemosphere* **2019**, *216*, 157–167. [CrossRef]
15. Zhao, W.; Zhou, Q.; Tian, Z.; Cui, Y.; Liang, Y.; Wang, H. Apply biochar to ameliorate soda saline-alkali land, improve soil function and increase corn nutrient availability in the Songnen Plain. *Sci. Total Environ.* **2020**, *722*, 137428. [CrossRef]
16. Organization for Economic Cooperation and Development. Test No. 222: Earthworm Reproduction Test (*Eisenia fetida*/*Eisenia andrei*). OECD Publishing. 2004. Available online: https://www.oecd.org/en/publications/test-no-222-earthworm-reproduction-test-eisenia-fetida-eisenia-andrei_9789264264496-en.html (accessed on 3 May 2024).
17. Ning, Y.C.; Jin, C.M.; Zhou, H.R.; Wang, E.Z.; Huang, X.N.; Zhou, D.X. Screening indices for cadmium—Contaminated soil using earthworm as bioindicator. *Environ. Sci. Pollut. Res.* **2018**, *25*, 32358–32372. [CrossRef]
18. Wang, J.H. Effects of Microplastics on Oxidative Stress Response and Carbon Source Utilization Intensity of Microbial Communities in Earthworms. Master's Thesis, Northeast Agricultural University, Harbin, China, 2022.
19. Rodríguez-Seijo, A.; Lourenço, J.; Rocha-Santos, T.A.P.; Costa, J.; Duarte, A.C.; Vala, H.; Pereira, R. Histopathological and molecularеffects of microplastics in *Eisenia andrei* Bouche. *Environ. Pollut.* **2017**, *220*, 495–503. [CrossRef]
20. Chen, Y.L.; Liu, X.N.; Leng, Y.F.; Wang, L. Defense responses in earthworms (*Eisenia fetida*) exposed to low-density polyethylene microplastics in soils. *Ecotoxicol. Environ. Saf.* **2020**, *187*, 109788. [CrossRef]

21. Forsell, V.; Saartama, V.; Turja, R.; Haimi, J.; Selonen, S. Reproduction, growth and oxidative stress in earthworm *Eisenia andrei* exposed to conventional and biodegradable mulching film microplastics. *Sci. Total Environ.* **2024**, *948*, 174667. [CrossRef]
22. Bradford, M.M. A rapid and sensitive method for the quantitation of microgram quantities of protein utilizing the principle of protein-dye binding. *Anal. Biochem.* **1976**, *72*, 248–254. [CrossRef] [PubMed]
23. Song, Y.; Zhu, L.S.; Wang, J.; Wang, J.H.; Liu, W.; Xie, H. DNA damage and effects on antioxidative enzymes in earthworm (*Eisenia foetida*) induced by atrazine. *Soil Biol. Biochem.* **2009**, *41*, 905–909. [CrossRef]
24. Fejes, P.; Kiricsi, I.; Lázár, K.; Marsi, I.; Rockenbauer, A.; Korecz, L. Attempts to produce uniform Fe (III) siting in Fe content SOD and LTA zeolites: An EPR and Mössbauer study. *Appl. Catal. A Gen.* **2003**, *242*, 63–76. [CrossRef]
25. Yang, Y.; Ji, F.; Cui, Y.; Li, M. Ecotoxicological effects of earthworm following long-term Dechlorane Plus exposure. *Chemosphere* **2016**, *144*, 2476–2481. [CrossRef]
26. Clark, A.G.; Dick, G.L.; Smith, J.N. Kinetic studies on a glutathione S-transferase from the larvae of *Costelytra zealandica*. *Biochem. J.* **1984**, *217*, 51–58. [CrossRef]
27. Xu, J.B.; Yuan, X.F.; Lang, P.Z. The determination of enzymic activity and its inhibition on catalase by ultraviolet spectrophotometry. *Environ. Chem.* **1997**, *16*, 73–76.
28. Zhang, W.; Liu, K.; Chen, L.; Chen, L.; Lin, K.; Fu, R. A multi-biomarker risk assessment of the impact of brominated flame retardant-decabromodiphenyl ether (BDE209) on the antioxidant system of earthworm *Eisenia fetida*. *Environ. Toxicol. Pharmacol.* **2014**, *38*, 297–304. [CrossRef]
29. Ellman, G.L.; Courtney, K.D.; Andres, V., Jr.; Featherstone, R.M. A new and rapid colorimetric determination of acetylcholinesterase activity. *Biochem. Pharmacol.* **1961**, *7*, 88–95. [CrossRef]
30. Kubota, R. Simultaneous Determination of Total Carbon, Nitrogen, Hydrogen and Sulfur in Twenty—Seven Geological Reference Materials by Elemental Analyser. *Geostand. Geoanal. Res.* **2009**, *33*, 271–283. [CrossRef]
31. Wu, W.; Xie, D.T.; Liu, H.B. Spatial variability of soil heavy metals in the three gorges area: Multivariate and geostatistical analyses. *Environ. Monit. Assess.* **2009**, *157*, 63–71. [CrossRef]
32. Zhou, D.X.; Ning, Y.C.; Wang, B.; Wang, G.D.; Su, Y.; Li, L.; Wang, Y. Study on the influential factors of Cd^{2+} on the earthworm *Eisenia fetida* in oxidative stress based on factor analysis approach. *Chemosphere* **2016**, *157*, 181–189. [CrossRef]
33. He, X.Q. *Applied Multivariate Statistical Analysis*; China Statistics Press: Beijing, China, 2010.
34. Tan, F.; Lu, Z. Study on the interaction and relation of society, economy and environment based on PCA–VAR model: As a case study of the Bohai Rim region. *China Ecol. Indic.* **2015**, *48*, 31–40. [CrossRef]
35. Liu, M.; Mu, J.; Wang, M.; Hu, C.; Ji, J.; Wen, C.; Zhang, D. Impacts of polypropylene microplastics on lipid profiles of mouse liver uncovered by lipidomics analysis and Raman spectroscopy. *J. Hazard. Mater.* **2023**, *458*, 131918. [CrossRef] [PubMed]
36. Dong, K.; Rao, Z.F.; Yang, X.Y.; Lin, J.C.; Zhang, P.X. Determination of several plastics by Raman spectroscopy. *China Plast. Ind.* **2011**, *39*, 67–70.
37. Zhi, Z.; Li, Y.; Liu, G.; Ou, Q. Identification and detection of label-free polystyrene microplastics in maize seedlings by Raman spectroscopy. *Sci. Total Environ.* **2025**, *958*, 178093. [CrossRef] [PubMed]
38. McCreery, R.L. *Raman Spectroscopy for Chemical Analysis*; John Wiley & Sons: New York, NY, USA, 2005.
39. Ren, L.; Liu, S.; Huang, S.; Wang, Q.; Lu, Y.; Song, J.; Guo, J. Identification of microplastics using a convolutional neural network based on micro-Raman spectroscopy. *Talanta* **2023**, *260*, 124611. [CrossRef] [PubMed]
40. Kaur, J.; Kelpsiene, E.; Gupta, G.; Dobryden, I.; Cedervall, T.; Fadeel, B. Label-free detection of polystyrene nanoparticles in Daphnia magna using Raman confocal mapping. *Nanoscale Adv.* **2023**, *5*, 3453–3462. [CrossRef] [PubMed]
41. Qin, D.; Kean, R.T. Crystallinity determination of polylactide by FT-Raman spectrometry. *Appl. Spectrosc.* **1998**, *52*, 488–495. [CrossRef]
42. Padermshoke, A.; Katsumoto, Y.; Sato, H.; Ekgasit, S.; Noda, I.; Ozaki, Y. Surface melting and crystallization behavior of polyhydroxyalkanoates studied by attenuated total reflection infrared spectroscopy. *Polymer* **2004**, *45*, 6547–6554. [CrossRef]
43. Yang, X.; Zhang, X.; Shu, X.; Xie, M.; Gong, J.; Fan, Y.; Li, Y.K.; Kai, J.R.; Ma, J. Reproduction, metabolic enzyme activity, and metabolomics in earthworms *Eisenia fetida* exposed to different polymer microplastics. *Ecotoxicol. Environ. Saf.* **2025**, *303*, 119018. [CrossRef]
44. Chen, L.; Liu, Z.; Yang, T.; Zhao, W.; Yao, Y.; Liu, P.; Jia, H. Photoaged tire wear particles leading to the oxidative damage on earthworms (*Eisenia fetida*) by disrupting the antioxidant defense system: The definitive role of environmental free radicals. *Environ. Sci. Technol.* **2024**, *58*, 4500–4509. [CrossRef]
45. Wang, H.; Xie, X.Y. Effects of combined pollution of Cd, Cu and Pb on antioxidant enzyme activities of earthworms. *China J. Environ. Sci.* **2014**, *35*, 2748–2754.
46. Gaetani, G.F.; Ferraris, A.M.; Rolfo, M.; Mangerini, R.; Arena, S.; Kirkman, H.N. Predominant role of catalase in the disposal of hydrogen peroxide within human erythrocytes. *Blood* **1996**, *87*, 1595–1599. [CrossRef]
47. Zhang, Q.; Zhu, L.; Wang, J.; Xie, H.; Wang, J.; Han, Y.; Yang, J. Oxidative stress and lipid peroxidation in the earthworm *Eisenia fetida* induced by low doses of fomesafen. *Environ. Sci. Pollut. Res.* **2013**, *20*, 201–208. [CrossRef]

48. Wang, J.; Coffin, S.; Sun, C.; Schlenk, D.; Gan, J. Negligible effects of microplastics on animal fitness and HOC bioaccumulation in earthworm *Eisenia fetida* in soil. *Environ. Pollut.* **2019**, *249*, 776–784. [CrossRef]
49. Wang, J.; Wang, J.; Wang, G.; Zhu, L.; Wang, J. DNA damage and oxidative stress induced by imidacloprid exposure in the earthworm *Eisenia fetida*. *Chemosphere* **2016**, *144*, 510–517. [CrossRef]
50. Li, L.L.; Feng, Y.Y.; Zhang, D.M.; Yang, C.F.; Xing, X.; Yuan, Z.Q.; Zhang, Z.C.; Zhang, X.Y. Cloning, bioinformatics and expression of StGST gene in potato against black scurf induced by sodium silicate. *China Veg.* **2025**, *1*, 77–87.
51. Pickett, C.B.; Lu, A.Y. Glutathione S-transferases: Gene structure, regulation, and biological function. *Annu. Rev. Biochem.* **1989**, *58*, 743–764. [CrossRef]
52. Zhao, L.; Zong, W.; Zhang, H.; Liu, R. Kidney toxicity and response of selenium containing protein-glutathione peroxidase (Gpx3) to CdTe QDs on different levels. *Toxicol. Sci.* **2019**, *168*, 201–208. [CrossRef]
53. Shu, Y.; Zhang, Y.; Cheng, M.; Zeng, H.; Wang, J. Multilevel assessment of Cry1Ab Bt-maize straw return affecting the earthworm *Eisenia fetida*. *Chemosphere* **2015**, *137*, 59–69. [CrossRef]
54. Ma, S. Research progress on glutathione peroxidase and glutathione transferase. *Prog. Vet. Med.* **2008**, *10*, 53–56.
55. Bamidele, J.; Idowu, A.; Ademolu, K.; Akinloye, O.; Bamgbola, A. Heavy metal accumulation and biochemical evaluation of earthworms from sawmills in Abeokuta, South-Western Nigeria. *Rev. De Biol. Trop.* **2015**, *63*, 1213–1221. [CrossRef]
56. Huang, L.L.; Liao, X.H.; Sun, H.; Jiang, X.; Liu, Q.; Zhang, L. Augmenter of liver regeneration protects the kidney from ischaemia—Reperfusion injury in ferroptosis. *J. Cell. Mol. Med.* **2019**, *23*, 4153–4164. [CrossRef] [PubMed]
57. Wang, J.Q. Research on the interaction between acetylcholinesterase of different species and organophosphorus pesticides based on homology modeling and molecular docking technology. *Agric. Technol.* **2024**, *44*, 26–31.
58. Zavala-Ocampo, L.M.; Aguirre-Hernández, E.; López-Camacho, P.Y.; Cárdenas-Vázquez, R.; Dorazco-González, A.; Basurto-Islas, G. Acetylcholinesterase inhibition and antioxidant activity properties of *Petiveria alliacea* L. *J. Ethnopharmacol.* **2022**, *292*, 115239. [CrossRef]
59. Han, Y.N.; Fu, M.R.; Wu, J.H.; Zhou, S.Q.; Qiao, Z.H.; Cheng, P.; Zhang, W.; Liu, F.; Ye, C.M.; Yang, J. Polylactic acid microplastics induce higher biotoxicity of decabromodiphenyl ethane on earthworms (*Eisenia fetida*) compared to polyethylene and polypropylene microplastics. *Sci. Total Environ.* **2023**, *862*, 160909. [CrossRef]
60. Zhang, J.; Meng, H.; Kong, X.; Cheng, X.; Ma, T.; He, H.; Du, W.C.; Yang, S.G.; Li, S.Y.; Zhang, L. Combined effects of polyethylene and organic contaminant on zebrafish (*Danio rerio*): Accumulation of 9-Nitroanthracene, biomarkers and intestinal microbiota. *Environ. Pollut.* **2021**, *277*, 116767. [CrossRef] [PubMed]
61. Yue, W.F.; Liu, J.M.; Li, G.L.; Li, X.H.; Wu, X.F.; Sun, J.T.; Sun, H.X.; Miao, Y.G. Effects of silkworm larvae powder containing manganese superoxide dismutase on immune activity of mice. *Mol. Biol. Rep.* **2008**, *35*, 513–517. [CrossRef]
62. Li, T.; Lu, M.; Xu, B.; Chen, H.; Li, J.; Zhu, Z.Z.; Yu, M.W.; Zheng, J.Y.; Peng, P.L.; Wu, S.J. Multiple perspectives reveal the gut toxicity of polystyrene microplastics on *Eisenia fetida*: Insights into community signatures of gut bacteria and their translocation. *Sci. Total Environ.* **2022**, *838*, 156352. [CrossRef]
63. Boots, B.; Russell, C.; Green, D. Effects of microplastics in soil ecosystems: Above and below ground. *Environ. Sci. Technol.* **2019**, *53*, 11496–11506. [CrossRef]
64. Baihetiyaer, B.; Jiang, N.; Li, X.X.; He, B.; Wang, J.; Fan, X.T.; Sun, H.M.; Yin, X.Q. Oxidative stress and gene expression induced by biodegradable microplastics andimidacloprid in earthworms (*Eisenia fetida*) at environmentally relevant concentrations. *Environ. Pollut.* **2023**, *323*, 121285. [CrossRef]
65. Ritschel, T.; Totsche, K.U. Modeling the formation of soil microaggregates. *Comput. Geosci.* **2019**, *127*, 36–43. [CrossRef]
66. Zhao, Z.Y.; Wang, P.Y.; Wang, Y.B.; Zhou, R.; Koskei, K.; Munyasya, A.N.S.; Liu, W.; Wang, Y.; Su, Y.; Xiong, Y.C. Fate of plastic film residues in agro-ecosystem and its effects on aggregate-associated soil carbon and nitrogen stocks. *J. Hazard. Mater.* **2021**, *416*, 125954. [CrossRef]
67. Six, J.; Elliott, E.T.; Paustian, K. Soil macroaggregate turnover and microaggregate formation: A mechanism for C sequestration under no-tillage agriculture. *Soil Biol. Biochem* **2000**, *32*, 2099–2103. [CrossRef]
68. Li, Q.; Bogush, A.; Van De Wiel, M.; Wu, P.; Holtzman, R. Microplastic polymer type impacts water infiltration and its own transport in soil. *iScience* **2025**, *28*, 113193. [CrossRef] [PubMed]
69. Zhang, G.S.; Zhang, F.X.; Li, X.T. Effects of polyester microfibers on soil physical properties: Perception from a field and a pot experiment. *Sci. Total Environ.* **2019**, *670*, 1–7. [CrossRef] [PubMed]
70. Yu, H.Y.; Ding, W.X.; Luo, J.F.; Donnison, A.; Zhang, J.B. Long-term effect of compost and inorganic fertilizer on activities of carbon-cycle enzymes in aggregates of an intensively cultivated sandy loam. *Soil Use Manag.* **2012**, *28*, 347–360. [CrossRef]
71. Anderson, A.S.M.; Chung, W.L.; Jennifer, T.; Werner, K.; Anika, L.; Roland, B.; Matthias, C.R. Impacts of microplastics on the soil biophysical environment. *Environ. Sci. Technol.* **2018**, *52*, 9656–9665. [CrossRef] [PubMed]
72. Liu, Y.; Wang, W.F.; He, J.Z. Microplastic effects on carbon cycling in terrestrial soil ecosystems: Storage, formation, mineralization, and microbial mechanisms. *Sci. Total Environ.* **2024**, *954*, 176658. [CrossRef]

73. Lu, C.; Qin, C.; Zhao, M.J.; Lu, C.X.; Zhao, L.X. Research progress on the toxic effects of antibiotics on earthworms. *Asian J. Ecotoxicol.* **2025**, *19*, 96–108.
74. Wang, F.; Yu, L.; Monopoli, M.P.; Sandin, P.; Mahon, E.; Salvati, A.; Dawson, K.A. The biomolecular corona is retained during nanoparticle uptake and protects the cells from the damage induced by cationic nanoparticles until degraded in the lysosomes. *Nanomed. Nanotechnol. Biol. Med.* **2013**, *9*, 1159–1168. [CrossRef]
75. Ruenraroengsak, P.; Novak, P.; Berhanu, D.; Thorley, A.J.; Valsami-Jones, E.; Gorelik, J.; Korchev, Y.E.; Tetley, T.D. Respiratory epithelial cytotoxicity and membrane damage (holes) caused by amine-modified nanoparticles. *Nanotoxicology* **2012**, *6*, 94–108. [CrossRef]
76. Sultan, M.; Wei, X.Y.; Duan, J.J.; Zhang, B.F.; Wu, M.F.; Cai, Z.X.; Pei, D.S. Comparative toxicity of polystyrene, polypropylene, and polyethylene nanoplastics on Artemia franciscana nauplii: A multidimensional assessment. *Environ. Sci. Nano* **2024**, *11*, 1070–1084. [CrossRef]
77. Lee, Y.K.; Murphy, K.R.; Hur, J. Fluorescence signatures of dissolved organic matter leached from microplastics: Polymers and additives. *Environ. Sci. Technol.* **2020**, *54*, 11905–11914. [CrossRef]
78. Meng, F.; Yang, X.; Riksen, M.; Geissen, V. Effect of different polymers of microplastics on soil organic carbon and nitrogen–A mesocosm experiment. *Environ. Res.* **2022**, *204*, 111938. [CrossRef] [PubMed]
79. Sun, Y.; Li, X.; Cao, N.; Duan, C.X.; Ding, C.F.; Huang, L.; Wanget, J. Biodegradable microplastics enhance soil microbial network complexity and ecological stochasticity. *J. Hazard. Mater.* **2022**, *439*, 129610. [CrossRef]
80. Li, C.; Cui, Q.; Li, Y.; Zhang, K.; Lu, X.Q.; Zhang, Y. Effect of LDPE and biodegradable PBAT primary microplastics on bacterial community after four months of soil incubation. *J. Hazard. Mater.* **2022**, *429*, 128353. [CrossRef]
81. Zhou, J.; Jia, R.; Brown, R.W.; Yang, Y.D.; Zeng, Z.H.; Jones, D.L.; Zang, H.D. The long-term uncertainty of biodegradable mulch film residues and associated microplastics pollution on plantsoil health. *J. Hazard. Mater.* **2023**, *442*, 130055. [CrossRef] [PubMed]
82. Zhang, X.L.; Xia, M.L.; Su, X.J.; Yuan, P.; Li, X.K.; Zhou, C.U.; Wan, Z.P.; Zou, W. Photolytic degradation elevated the toxicity of polylactic acid microplastics to developing zebrafish by triggering mitochondrial dysfunction and apoptosis. *J. Hazard. Mater.* **2021**, *413*, 125321. [CrossRef] [PubMed]

Disclaimer/Publisher's Note: The statements, opinions and data contained in all publications are solely those of the individual author(s) and contributor(s) and not of MDPI and/or the editor(s). MDPI and/or the editor(s) disclaim responsibility for any injury to people or property resulting from any ideas, methods, instructions or products referred to in the content.